frontiers | Frontiers in Biomaterials Science

TYPE Original Research
PUBLISHED 09 May 2024
DOI 10.3389/fbiom.2024.1365781

OPEN ACCESS

EDITED BY
Jenny Robinson,
University of Washington, United States

REVIEWED BY
Sushma Venkata Mudigunda,
Harvard Medical School, United States
Zalike Keskin Erdogan,
Imperial College London, United Kingdom

*CORRESPONDENCE
Kaitlin C. Fogg,
kaitlin.fogg@oregonstate.edu

RECEIVED 04 January 2024
ACCEPTED 15 April 2024
PUBLISHED 09 May 2024

CITATION
Cadena IA, Adhikari G, Almer A, Jenne M, Obasi N, Soria Zurita NF, Rochefort WE, Mueller JL and Fogg KC (2024), Development of a 3D *in vitro* human-sized model of cervical dysplasia to evaluate the delivery of ethyl cellulose-ethanol injection.
Front. Biomater. Sci. 3:1365781.
doi: 10.3389/fbiom.2024.1365781

Development of a 3D *in vitro* human-sized model of cervical dysplasia to evaluate the delivery of ethyl cellulose-ethanol injection

Ines A. Cadena[1], Gatha Adhikari[2], Alyssa Almer[1], Molly Jenne[1], Ndubuisi Obasi[1], Nicolas F. Soria Zurita[3], Willie E. Rochefort[1], Jenna L. Mueller[2,4,5] and Kaitlin C. Fogg[1]*

[1]School of Chemical, Biological, and Environmental Engineering, Oregon State University, Corvallis, OR, United States, [2]Department of Bioengineering, University of Maryland, College Park, MD, United States, [3]School of Engineering Design and Innovation, College of Engineering, Pennsylvania State University, University Park, PA, United States, [4]Department of OB-GYN and Reproductive Science, University of Maryland School of Medicine, Baltimore, MD, United States, [5]Marlene and Stewart Greenebaum Cancer Center, University of Maryland School of Medicine, Baltimore, MD, United States

Introduction: Cervical cancer, the second leading cause of cancer-related death for women worldwide, remains a preventable yet persistent disease that disproportionately affects women in low and middle-income countries (LMICs). While existing therapies for treating cervical dysplasia are effective, they are often inaccessible in LMICs. Ethanol ablation is an alternative low-cost, accessible therapy that we previously enhanced into ethyl cellulose (EC)-ethanol gel formulation to improve efficacy.

Methods: To evaluate the efficacy of EC-ethanol, in this study, we developed a 3D *in vitro* model of cervical dysplasia featuring a central lesion of cervical cancer cells surrounded by fibroblasts and keratinocytes. Using a GelMA hydrogel formulation (8.7% w/v), we successfully built a 3D model that captured the architectural complexity of cervical dysplasia. We evaluated changes in cell coverage and cell viability. Then, we compared the viscoelastic properties of the GelMA hydrogels to human cervical tissue and using micro-CT imaging, we assessed EC-ethanol injection deposition in the hydrogel, revealing retention of virtually the entire injected volume near the injection site. Finally, we measured changes in cell viability and cell coverage after the EC-ethanol injection.

Results: The developed 3D in vitro model successfully replicated the architectural complexity of cervical dysplasia, demonstrating high cell viability and capturing cell responses effectively. The GelMA hydrogel formulation (8.7% w/v) exhibited viscoelastic properties akin to human cervical tissue. Micro-CT imaging revealed efficient deposition of EC-ethanol within the hydrogel, with retention of the injected volume near the injection site. Furthermore, the EC-ethanol injection significantly reduced cervical cancer cell viability and cell coverage while preserving healthy cells within the model.

Conclusion: Our findings indicate that our 3D *in vitro* model mirrored the architecture of cervical dysplasia and demonstrated the potential of EC-ethanol for localized treatment of cervical dysplasia.

KEYWORDS

hydrogel, cervical dysplasia, triculture, GelMA, ethanol ablation, ethyl cellulose

1 Introduction

Cervical cancer is a preventable disease, yet it remains the second leading cause of cancer-related death for women worldwide (Ferlay et al., 2015). Mortality is projected to rise to 400,000 annual deaths by 2030, and 90% of those deaths will be in low and middle-income countries (LMICs) if no additional action is taken (Ferlay et al., 2015). Cervical cancer is highly preventable through vaccination against the human papillomavirus (HPV) (Human papillomavirus vaccines, 2015), as well as screening, diagnosis, and treatment of cervical dysplasia before it progresses to cervical cancer (Comprehensive Cervical Cancer Control, 2014). While considerable efforts have been made to increase access to vaccination, screening, and diagnosis (Jeronimo et al., 2005; Huchko et al., 2014; Huchko et al., 2015; Lam et al., 2015; Mueller et al., 2017; Mueller et al., 2018), up to 80% of women who have been diagnosed with cervical dysplasia in LMICs never receive treatment, largely due to treatment being inaccessible at the point of care (Gage et al., 2003). Thus, there is a need to develop novel therapies for cervical dysplasia that are accessible in LMICs.

In light of the above, ethanol ablation is a form of clinical tissue ablation well-suited for LMICs (Path, 2013). Ethanol ablation entails directly injecting ethanol into the region of interest to induce necrosis through protein denaturation and cytoplasmic dehydration (Tsu et al., 2013). It is a standard treatment option for small, unresectable liver tumors and has low complication rates (Abdul-Karim et al., 1982). However, its direct injection into tissue leads to fluid leakage outside of the lesion, which decreases efficacy and can lead to side effects (Seki et al., 1989). To address this limitation, we develop a new formulation that includes a low-cost, biocompatible polymer called ethyl cellulose (EC) that forms a gel when injected into tissue. Previous studies have shown promising results in the use of EC-ethanol ablation to safely and effectively treat tumors in a variety of preclinical models, including a chemically induced hamster cheek pouch model of squamous cell carcinoma (Morhard et al., 2017) and subcutaneous flank tumor induced by injecting a murine breast cancer cell line (Nief et al., 2021). While we are most interested in applications in the cervix, these other models were used as no xenograft models of cervical dysplasia currently exist (Larmour et al., 2015). Most recently, we scaled up to swine cervices, which are comparable in size to human cervices (Lorenzen et al., 2015). However, currently, no swine model of cervical dysplasia exists—thus, our previous study was limited to normal anatomy. Taken together, none of these widely used animal models recapitulate the microenvironment of cervical dysplasia or cervical cancer, limiting our ability to investigate how to tune EC-ethanol ablation such that it kills precancerous and cancerous cells and leaves the surrounding healthy cells alone.

Three-dimensional (3D) *in vitro* models offer potential avenues for investigating the therapeutic application of EC-ethanol ablation in the context of cervical dysplasia. However, current models, including a 3D printed model (Larmour et al., 2015) and an organotypic raft culture (De Gregorio et al., 2020), lack suitability for testing EC-ethanol injection due to their inability to capture cervical dysplasia's histology and size. In a prior study, we successfully demonstrated that using gelatin methacrylate (GelMA) as the main component in a 3D *in vitro* model allowed phenotypic cell responses that captured the histology of the tumor microenvironment (Cadena et al., 2023). The motivation for using GelMA in designing a 3D *in vitro* model for cervical dysplasia is inspired by its favorable characteristics established in previous studies, showing its biocompatibility, tunable mechanical properties, and support for cell adhesion, proliferation, and differentiation (Nichol et al., 2010). Previous studies have demonstrated the efficacy of GelMA hydrogels in facilitating the growth and function of various cell types (Van Den Bulcke et al., 2000), including fibroblasts and epithelial cells, which are crucial components of the cervical microenvironment. Additionally, their suitable rheological properties enable the fabrication of complex 3D structures, mimicking the architectural complexity of cervical dysplasia *in vitro* (Bogorad et al., 2015). Moreover, GelMA hydrogels possess good transport properties, allowing for the diffusion of essential nutrients and oxygen necessary for cell viability and function in 3D culture systems (Belair and Abbott, 2017). Owing to these properties, the use of GelMA in constructing a 3D *in vitro* model for cervical dysplasia offers a promising approach to mimic the ECM environment and cellular interactions characteristic of the disease, thus facilitating the evaluation of potential therapeutic interventions. In our previous 3D model for cervical cancer, GelMA was observed to support cervical cancer progression after 48 h of coculture with endothelial cells (Cadena et al., 2023). Despite its success in modeling cervical cancer, our 3D model reflected characteristics of metastatic cancer and is, therefore, unsuitable for studying cervical dysplasia. Additionally, the model's construction in a 96-well plate restricted its size, rendering it ill-suited for testing treatments such as the EC-ethanol injection. Nevertheless, considering GelMA's mechanical properties (Yue et al., 2015), it remains a promising scaffold for developing a 3D *in vitro* model specifically tailored for cervical dysplasia with some tuning for the test of therapies involving EC-ethanol injection.

The overall goal of the present study was to develop a 3D *in vitro* model of cervical dysplasia that shows an initial stage of cervical cancer invasion for the application of an EC-ethanol injection to target cervical cancer growth and viability over time. We developed a 3D triculture model that is the approximate size of a human cervix, captured cell responses, and resembled the mechanical properties of human cervical tissue. We then administered EC-ethanol to the 3D model and demonstrated that we could cause necrosis of the cancer cells in the center of the model while leaving the noncancerous cells (fibroblasts and keratinocytes) on the outside of the model alive. Overall, this study demonstrated that our 3D model captured the architecture and geometry of the cervical disease and could be used to evaluate the potential of EC-ethanol (and, in the future, other novel therapies) for localized treatment of cervical dysplasia.

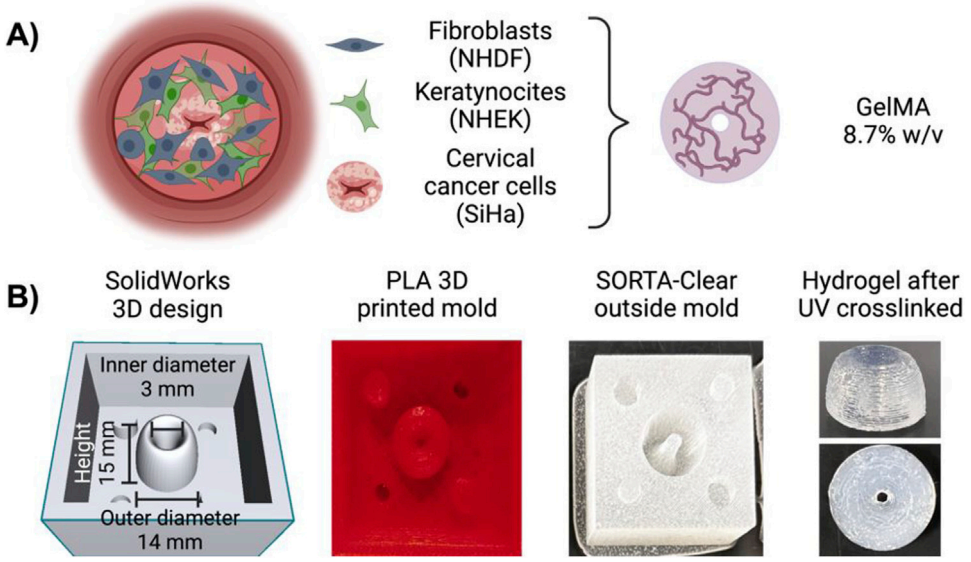

FIGURE 1
Three-dimensional (3D) mold for a tri-coculture model of cervical dysplasia. **(A)** Schematic representation of the 3D model with cervical cancer cells (SiHa) in the center encapsulated in Ge1MA (8.7%w/v with LAP), surrounded by fibroblasts (NHDF) cells suspended in Ge1MA (8.7%w/v with LAP), and covered with keratinocytes (NHEK) cells suspended in culture media. **(B)** The outside mold was created in SolidWorks, printed in PLA with a 10% infill, and built with SORTA-Clear 40 silicone rubber. Diagram created in BioRender.com.

2 Materials and methods

2.1 Cell lines and reagents

Normal adult human dermal fibroblasts (NHDF-Ad) and human epidermal keratinocytes-adult (NHEK-Ad) were purchased from Lonza (CC-2511 Walkerville, MD), and SiHa cells were purchased from ATCC (ATCC® HTB-35™, Manassas, VA). All cell lines were used without additional characterization. NHDF cells were cultured in FBM fibroblast basal media (supplemented with FGM-2 SingleQuot supplements: insulin, hEGF-B, GA-1000, and FBS) (Lonza). NHEK cells were expanded in KBM gold basal medium (KGM gold supplemented with Lonza's SingleQuot supplements: hydrocortisone, transferrin, epinephrine, GA-1000, BPE low protein-nonspecific, hEGF, and recombinant human insulin 0.5%) (Lonza). Human cervical cancer cell line SiHa from ATCC (ATCC® HTB-35™, Manassas, VA) was used without additional characterization. SiHa cells were expanded in Eagle's Minimum Essential Medium (EMEM, ATCC), supplemented with 10% FBS (Sigma-Aldrich, St. Louis, MO) and 1% Penicillin-Streptomycin (P/S, Sigma-Aldrich). All cell lines were expanded in standard cell culture conditions (37°C, 21% O_2, 5% CO_2) until passage 5. Cells were recovered at 80% confluency.

2.2 Cell staining and evaluation of cell response

All reagents were purchased from ThermoFisher (Waltham, MA) unless stated. The cell area was evaluated by taking images of the cells over time. NHDF cells, NHEK cells, and SiHa cells were stained with fluorescent dyes. CellTracker Green CMFDA (C7025), CellTracker Blue CMF2HC (C12881), and CellTracker Red CMTPX (C34552) were used to visualize and quantify the cell area over time. Three channels (469/525 nm, 628/685 nm, and 377/447 nm excitation/emission) with 9 z-stack images were taken every 12 h for 48 h using a Cytation 5 cell imaging multimode reader (Agilent Technologies). The distance between the z-stack is described in each experiment. Images were processed with NIH Fiji- ImageJ, and cell coverage was measured by calculating the area within the well covered by cells and dividing it by the total well area (NIH, Bethesda, MD). Cell viability was quantified by adding Calcein AM (2M, eBioscience™ Calcein AM Viability Dye, 65-0853-39, San Diego, CA) and Propidium Iodide (5M Propidium Iodide Ready Flow™ Reagent, R37169) to the cell cultures. Following the manufacturer's instructions, the staining solution was added on top of the wells at either 24 h or 48 h post-cultured or post-treatment. Two-channel (469/525 nm and 586/647 excitation/emission) 54.8 µm z-stack and 180 µm z-stack images in a 4 × 4 and 4 × 5 montage were taken to image the 3D *in vitro* models. Images were stitched to facilitate the image analysis and quantification of live/dead cells. The mean fluorescent intensity (MFI) of live cells (stained with calcein AM) and dead cells (stained with propidium iodide) were quantified using Fiji ImageJ, and the number of cells that were alive or dead was quantified using Gen 5 software (Agilent Technologies).

2.3 Design of a 3D mold

We employed SolidWorks (Dassault Systèmes SolidWorks Corporation) to create a customized 3D mold that mirrors the size and histology of cervical dysplasia, featuring cancer cells on the inside and surrounded by healthy cells on the outside (Figure 1A).

TABLE 1 Cell density in the 10 mm and 15 mm constructs. The cells' pellet was dissolved in culture media, and then cells were suspended in GelMA (8.7%w/v) hydrogels.

Model thickness (mm)	NHDF (cells/well)	NHEK (cells/well)	SiHa (cells/well)
10	53,333	83,160	26,667
15	1,33,333	277,200	106,667

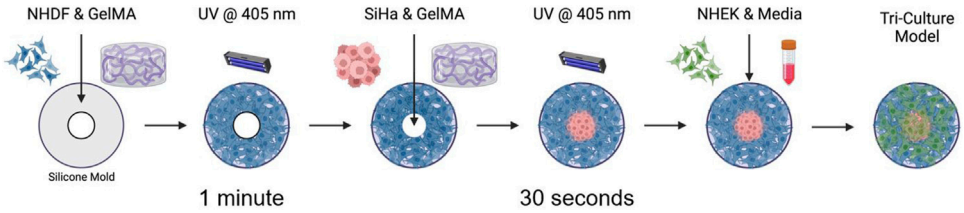

FIGURE 2
Fabrication of a 3D triculture hydrogel model for cervical dysplasia. Schematic illustrating fabrication process of the 3D tri-culture model. Fibroblasts (NHDF), are first recovered from the culture plates and suspended in Ge1MA (8.7% w/v with LAP). 1.5 mL of cell: hydrogel solution is added to the silicone mold and UV form 1 min. Then the construct is carefully added to the 24-well plate ibidi, immediately after cervical cancer cells (SiHa) are recovered from culture plates and suspended in GelMA (8.7% w/v with LAP). Cancer cell-hydrogel solution is pipetted in the center of the 3D model (–200 !IL), and UV cured for about 30 s. Finally, keratinocytes (NHEK) are recovered from the culture plates, the cell pellet is mixed with culture media and added on top of the final 3D model. Constructs are incubated at 37°C for the duration of the experiment. Diagram created in BioRender.com.

Using polylactic acid (PLA) material with 10% infill, the mold was 3D printed at the Valley Library at Oregon State University. Subsequently, we filled the PLA mold with SORTA-Clear 40 silicone rubber (Smooth-ON, Inc., Macungie, PA 18062). Following the manufacturer's guidelines, the mold was then cured and sterilized (Figure 1B). This was done for two sizes, one with a height of 10 mm, and inner diameter of cervical dysplasia of 2 mm, and another with a height of 15 mm and inner diameter of 3 mm. Both models had an outside diameter of 14 mm (Supplementary Figure S1).

2.4 Assembly of 3D tri-culture model of cervical dysplasia

We have previously reported a multilayer model of cervical cancer that used 7% w/v gelatin methacrylate (GelMA) to promote cervical cancer invasion over time (Cadena et al., 2023). Previous viscoelastic experiments showed a closer mimic of the elastic properties of GelMA at 8.7% to the human cervix compared to our previous model (GelMA 7%w/v) (Supplementary Figure S2). GelMA at 8.7% w/v also gives us the possibility to improve the hydrogel formulation for future studies where the inclusion of extracellular matrix components is possible at this GelMA concentration. We prepared the GelMA hydrogels at a final concentration of 8.7% w/v following manufacturer instructions (GelMA, AdvancedBiomatrix, San Diego, CA). We used lithium pheny-2,4,6-trimethylbenzoylphosphinate (LAP) as a photoinitiator (17 mg/mL, Advanced Biomatrix), as it has been reported to improve cell viability compared to irgacure (Xu et al., 2020; Montazerian et al., 2021). NHDF cells were suspended in an 8.7% w/v GelMA with LAP solution to the desired cell density for each model (1.5 mL of cell: hydrogel solution, 400 µL of NHDF cells were suspended in 1.5 mL of GelMA) (Table 1). For the 10 mm construct, we use approximately 500 µL of the final solution, and for the 15 mm construct, we use 1.5 mL of the solution. The solution was pipetted into the silicone mold and UV-cured using a 405 nm light for 1 min, following the protocol specified by the manufacturer. The hydrogel was then removed from the mold and carefully added to a black-walled 24-µ plate (IBIDI, Fitchburg, WI). Following a similar procedure, SiHa cells were suspended in a GelMA hydrogel (8.7% w/v) at the desired cell density (Table 1). The mixture was then pipetted in the center of the well and UV crosslinked for 30 s using the same light source as before (10 mm construct used about 100 µL, and 15 mm construct 250 µL of cell-hydrogel solution, 400 µL of SiHa cells were suspended in 1.5 mL of GelMA). Lastly, 120 µL (10 mm) or 300 µL (15 mm) NHEK cells suspended in KBM-KGM culture media were added on top to simulate normal epithelium. Constructs were covered in 100 µL of culture media comprised of a 1:1:1 ratio of FBM-FGM-2, KBM-KGM, and EMEM. The media was changed every 24 h, and the plate was incubated at 37°C and 5% CO_2 in a BioSpa live cell analysis system (Agilent Technologies, Santa Clara, CA) for 48 h (Figure 2).

2.5 Tissue preparation and comparison of material properties between human cervix samples and GelMA hydrogel

Supplied by the University of Maryland School of Medicine (UMSOM) post-autopsy, human cervix samples were dissected to remove excess fat and residual tissue (Supplementary Figure S3). For rheometric testing, the cervix was sectioned laterally to obtain samples that fit the 25 mm circular plate of the AR-G2 rheometer (TA Instruments, New Castle, DE). They were stored

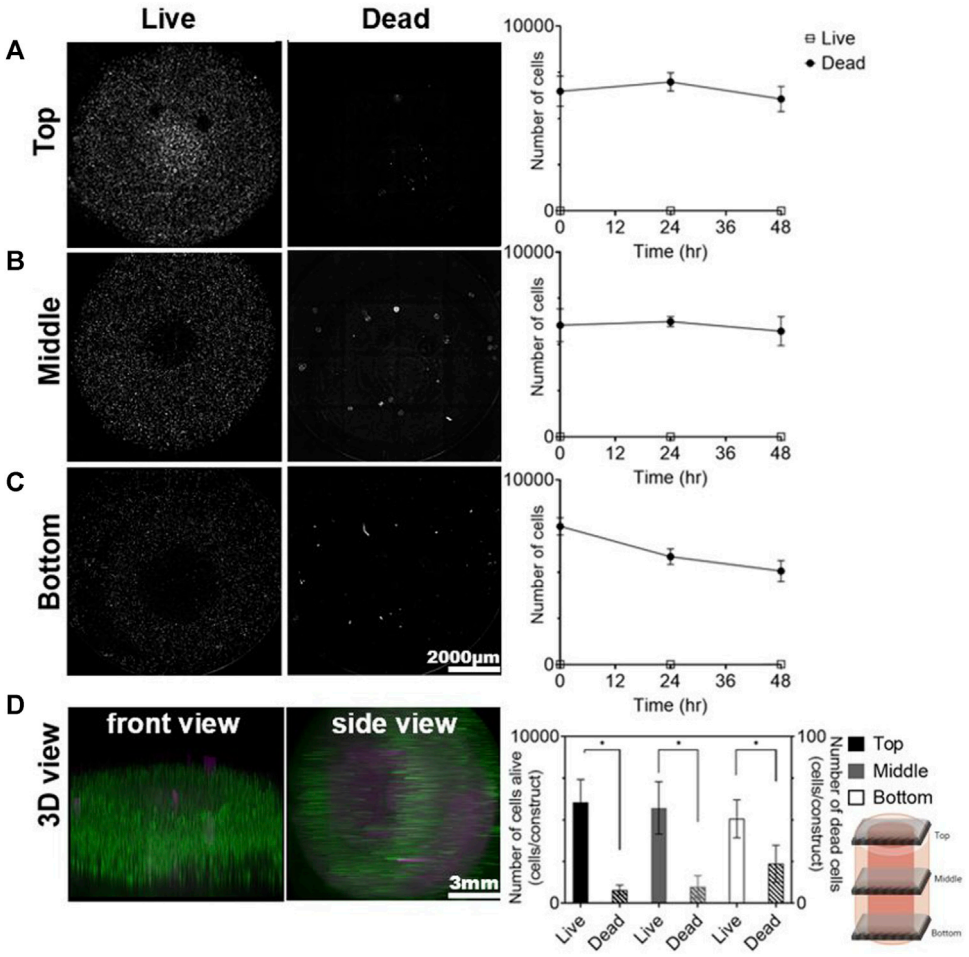

FIGURE 3
Cell viability in the 3D model for cervical dysplasia. Cell viability was measured by quantifying the number of live and dead cells in the **(A)** top, **(B)** middle, and **(C)** bottom layers of the construct at 0, 24, and 48 h of culturing. Cells were stained with a Calcein and Propidium Iodide solution at every time point. Top layer corresponded to the images at the z-stacks = 493.2-274 gm, the middle layer the z-stacks = 109.6–219.2 gm, and the bottom layer were at a z-stacks = -54.8-54.8 gm. Z-projections of the top, middle, and bottom layer were created to quantify the number of cells per construct. One z-stack image was added below the focused point and 8 slices were added above the focus point. Distance between z-stack layers was defined as 54.8 gm. **(D)** A 3D view of the live cells (green-calcein) and dead cells (magenta-propidium iodide) was created using Fiji ImageJ. Images represent 48 h after culturing. A montage of 4 × 4 (rows x columns) with 9 z-stacks were taken to capture the 3D model. The sample thickness was 493.2 gm, and the scale bar was set at 2000 gm. Images were created using Gen5 V3.14 software and Fiji-ImageJ. The data represent the mean ± SEM (n = 4). *$p < 0.05$, analyzed using 2-Way ANOVA with Tukey post-test.

in 10% PBS and incubated at 37°C for 1 h before experiments. Likewise, the GelMA hydrogels were crosslinked with LAP using a 405 nm light source for about 1 min; then, they were also incubated at 37°C for 1 h to accurately depict the mechanical properties of the model. We characterized the mechanical properties of our GelMA hydrogels relative to human cervical tissue using a previously described method (Cadena et al., 2023). Briefly, a dynamic oscillatory shear measurement was used to evaluate the rheological properties of GelMA at 8.7% w/v (Supplementary Figure S3). GelMA was kept in the incubator at 37°C before reading. Rheological characterization was evaluated using an AR-G2 rheometer (TA Instruments, New Castle, DE) equipped with a 20 mm standard steel parallel top plate with a bottom standard Peltier plate. 150 grit (120 μm particle size) sandpaper was attached to the top and bottom to prevent hydrogel from slipping. Frequency sweeps were set from 0.01 to 10 rad/s within the linear viscoelastic (LVE) region. The temperature of 37°C and a strain amplitude of 5% were kept constant during analysis. The hydrogels were allowed to equilibrate to the plate temperature for 15 min before frequency sweeps. The rheological parameters (storage moduli (G′), loss moduli (G") and their ratio (G'/G") were determined from these experiments.

2.6 EC-ethanol formulation and contrast agent for visualization

Mixtures of ethyl cellulose (Sigma Aldrich, St. Louis, MO) and ethanol (200 proof, Koptec, King of Prussia, PA) were prepared at room temperature using a hotplate stirrer (VWR Hotplate/Stirrer). The ethyl cellulose and ethanol mixture (EC-ethanol) were continuously stirred

until the ethyl cellulose was completely dissolved. In all experiments, EC concentrations of 12% (EC to ethanol, % weight: volume) were used, as previous studies indicated significant increases in distribution volume for ≥6% EC (Adhikari et al., 2023). To contrast the CT image between the injectate and surrounding cell construct, iohexol (Omnipaque, GE Healthcare, Chicago IL) was added to EC-ethanol. Iohexol was chosen for its high solubility in ethanol. The EC-ethanol-iohexol solutions were injected into the cell constructs and imaged using micro-CT (Bruker SkyScan 1276, Billerica, MA) as previously described (Adhikari et al., 2023). An 80 mg/mL concentration of iohexol was used for all experiments based on previous study results that maximized the signal-to-background ratio.

2.7 Micro-CT imaging

The Bruker SkyScan 1276 micro-CT was employed for imaging to visualize the EC-ethanol distribution. Samples were positioned upright during imaging, with the needle insertion site oriented at the 12 o'clock position. The images had a pixel size of 81.072 μm, a field of view of 9.31 × 158.75 cm, and were acquired in full rotation (360°) in a 504 × 336 matrix. After image acquisition and reconstruction, post-alignment correction and appropriate ring correction were applied. EC-ethanol distribution volume was then quantified within the hydrogel by loading the images onto 3Dslicer software (Kitware, Clifton Park, NY) and maximum entropy auto-thresholding was applied to the data to segment EC-ethanol-iohexol (Muñoz et al., 2021).

2.8 EC-ethanol injection in 3D triculture hydrogel model

We evaluated the effect of an EC-ethanol injection (EC to ethanol, weight to weight, i.e., 12% EC to 88% pure ethanol) on cell viability and cancer cell area in the 3D *in vitro* model. Using the 15 mm thickness construct, we cocultured the 3 cell lines for 24 h at 37°C and 5% CO_2 in the BioSpa. Then, 50 μL of 12% EC-ethanol was injected into the 3D *in vitro* model at a needle depth of 7 mm using a 22 G syringe. Culture media was changed every 24 h, and images were taken using the same procedure described above. Two-channel and three-channel 180 μm z-stack images were taken every 12 h for 48 h post-injection to evaluate changes in cell viability and cancer cell area over time. Finally, to examine the accurate placement of the ethyl-cellulose drug within the 3D *in vitro* model, we employed bright-field imaging using a Cytation 5 cell imaging multimode reader (Agilent Technologies). Images were stitched and z-projected prior to analysis of the MFI and SiHa cell area. As a control for cell viability, the 3D models were submerged in ethanol (99% v/v) for 48 h.

2.9 Statistical analysis

All quantitative measures are expressed as mean ± standard deviation or as median and interquartile range (if an approximate normal distribution was not achieved after an appropriate transformation). Statistical analysis was performed using a two-way analysis of variance (ANOVA) with Tukey correction for multiple comparisons or one-way ANOVA when appropriate. The same analysis was used to compare human cervices samples to the GelMA hydrogels. All statistical analyses were performed using Prism 8.2.1 software (GraphPad, San Diego, CA); *p*-values less than 0.05 were considered statistically significant. Replicates are specified in each experiment, and asterisks denote significance.

3 Results

3.1 Cell viability and cell coverage in 3D *in vitro* models of cervical dysplasia

We quantified the number of live *versus* dead cells in the 3D model during 48 h of culture and saw that, over time, cell viability was maintained throughout the 3D model (Figure 3). There were no significant differences in cell viability as a function of z-position. However, there was a slight decrease in the number of viable cells in the bottom layer at 24 h (Figure 3C). The 15 mm construct followed similar trends (Supplementary Figure S4).

Our 3D model captured the architecture and geometry of cervical dysplasia, with SiHa cells in the center and healthy fibroblasts and keratinocytes surrounding them. We evaluated changes in cell area over time (Figure 4; Supplementary Figure S4). At time 0 h, cell coverage was highest for SiHa cells on the inside, and the outside had higher coverage of NHDF cells and NHEK cells. After 48 h of culturing, there was an increase in NHEK coverage on the inside, and NHDF cells moved slightly to the inside. However, at 48 h, SiHa cells remained the predominant cell type in the inside region, and NHDF cells were predominant in the outside region (Figure 4B). NHEK and NHDF cells increased their cell coverage over time, while SiHa cells maintained constant cell coverage throughout the construct after 48 h (Figure 4C). The 15 mm model has demonstrated the same trends (Supplementary Figure S4). Overall, these results showed that after 48 h of culturing, the cells were viable throughout the model and mimicked the size and architecture of cervical dysplasia.

3.2 Comparison of material properties between the human cervix and GelMA hydrogels

To ensure that the biophysical properties of our 3D model matched the tissue we were trying to recapitulate, we characterized the mechanical properties of our GelMA hydrogels relative to human cervical tissue (Figure 5). Our 8.7% w/v GelMA had very similar storage moduli compared to human cervices, indicating that it captured the elastic contribution of cervical tissue's resistance to deformation (Figure 5C). The loss moduli of the GelMA were lower, suggesting that we may need to add in additional ECM proteins or explore a wider range of GelMA hydrogel formulations to capture elastic and viscous contributions (Figure 5D). Our results had a higher G'/G″ value for the GelMA hydrogels, suggesting its greater elasticity than the human cervical tissue (Figure 5E).

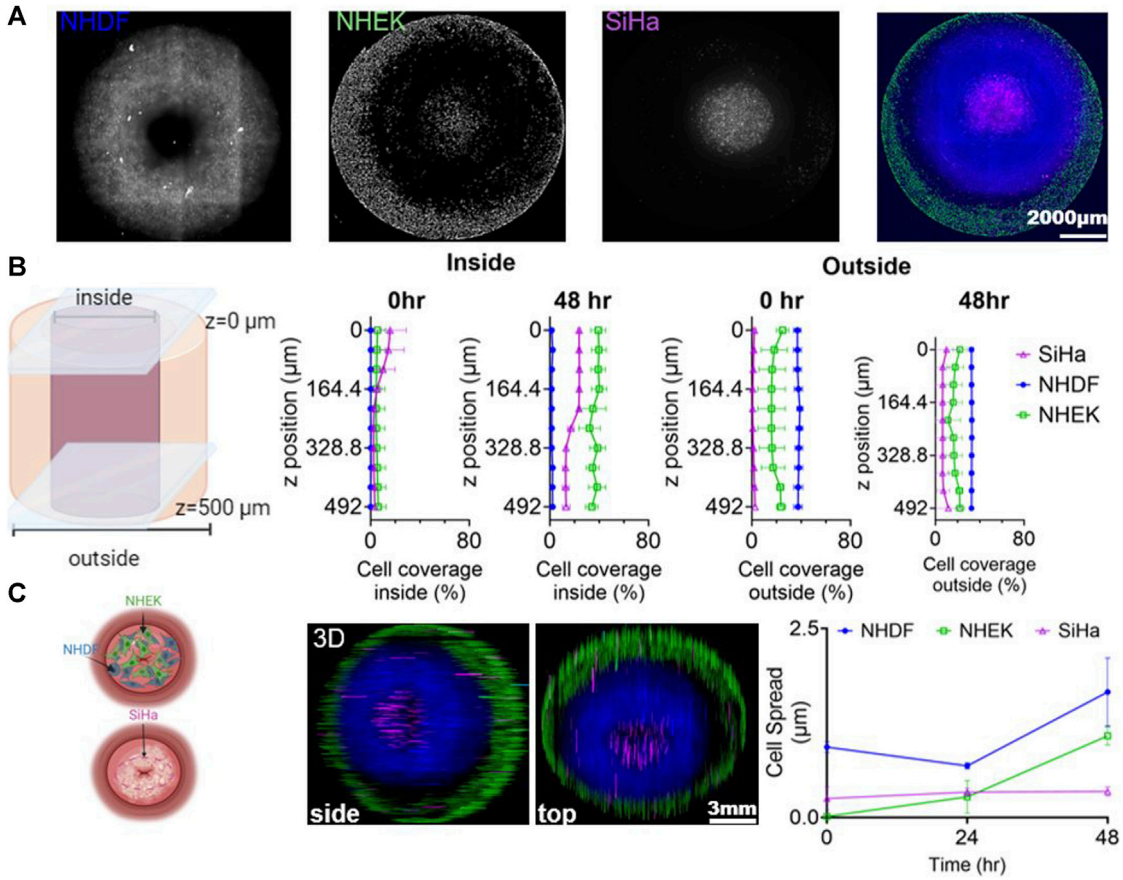

FIGURE 4
Phenotypic Cell Response in Cervical Dysplasia 3D *in vitro* Model. **(A)** Representative z-projection of the images of the 3 cell lines (NHDF (blue), NHEK (green), and SiHa (magenta)) after 48 h of culturing in the 3D model. **(B)** Representation of the outer and inner regions of the 3D model, with cell coverage quantification along the *z*-axis. **(C)** Schematic representation of the 3D model with a view of the cells after 48 h of co-culture. Cell spread was tracked by staining NHDF cells with CellTracker Green CMFDA (C7025), SiHa were tracked using CellTracker Red CMTPX (C34552), and NHEK cells with CellTracker Blue CMF2HC (C 12881). Cell spread was measured as the area covered by each cell line. Data was normalized to the time 0 and showed as a fraction. The 3D hydrogel model was cultured in a 24-well ibidi plate for 48 h, with media changed every 24 h. A montage of 4 x 4 with 54.8 z-stacks was taken to capture the 3D model. Images were created and processed with GenS V3.14 software. 3D z-projections and color of the images were defined and generated using Fiji ImageJ (showing the side and bottom view). Cell area was measured using Fiji ImageJ. Data represent the mean ± SD (n = 3). Schemes created in BioRender.com.

3.3 Micro-CT imaging to visualize the distribution of the injectate

GelMA hydrogels (8.7% w/v) were injected with EC-ethanol-iohexol (using injection parameters optimized in a previous study) (Adhikari et al., 2023). Using Micro-CT imaging, we evaluated if iohexol (Figure 6B) correlated with where the EC-ethanol injectate went, which could be visualized by its white color against the translucent GelMA background (once the GelMA was sectioned in half) (Figure 6A). We demonstrated that there were no statistical differences between the two visualization methods (Figure 6D), which in the future will enable us to track where the gel forms in our intact 3D *in vitro* models without the need for sectioning. Moreover, our results indicated that for injected volumes of 50 uL, virtually the entire injected volume was retained near the site of injection (Figure 6C). This not only facilitates comprehensive visualization but also empowers precise quantitative analysis of the distribution of EC-ethanol in our *in vitro* constructs.

3.4 Effect of ethyl cellulose-ethanol injection on cell viability and cell area in 3D *in vitro* model

In our 3D *in vitro* model, we evaluated the efficacy of the EC-ethanol injection in reducing the cell viability of the SiHa cells and preserving the viability of the surrounding healthy cells (Figure 7). We injected 50 μL of EC-ethanol and evaluated cell viability in the 3D model compared to positive and negative controls. The 3D models cultured in media had viable cells throughout the construct with very few dead cells (Figure 7A). In contrast, the 3D models submerged in ethanol had only dead cells (Figure 7B). Finally, the 3D models injected with the EC-ethanol had higher cell viability outside the EC-injection and higher cell death in the injection area (Figure 7C).

We then evaluated the ability of the EC-ethanol injection to reduce the SiHa cell area, as the goal in patients would be to eliminate the spread of cancer cells to the surrounding healthy tissue (Figure 8). NHDF, NHEK and SiHa cells were stained with cell tracker dies and cultured in the 3D model for 24 h prior to

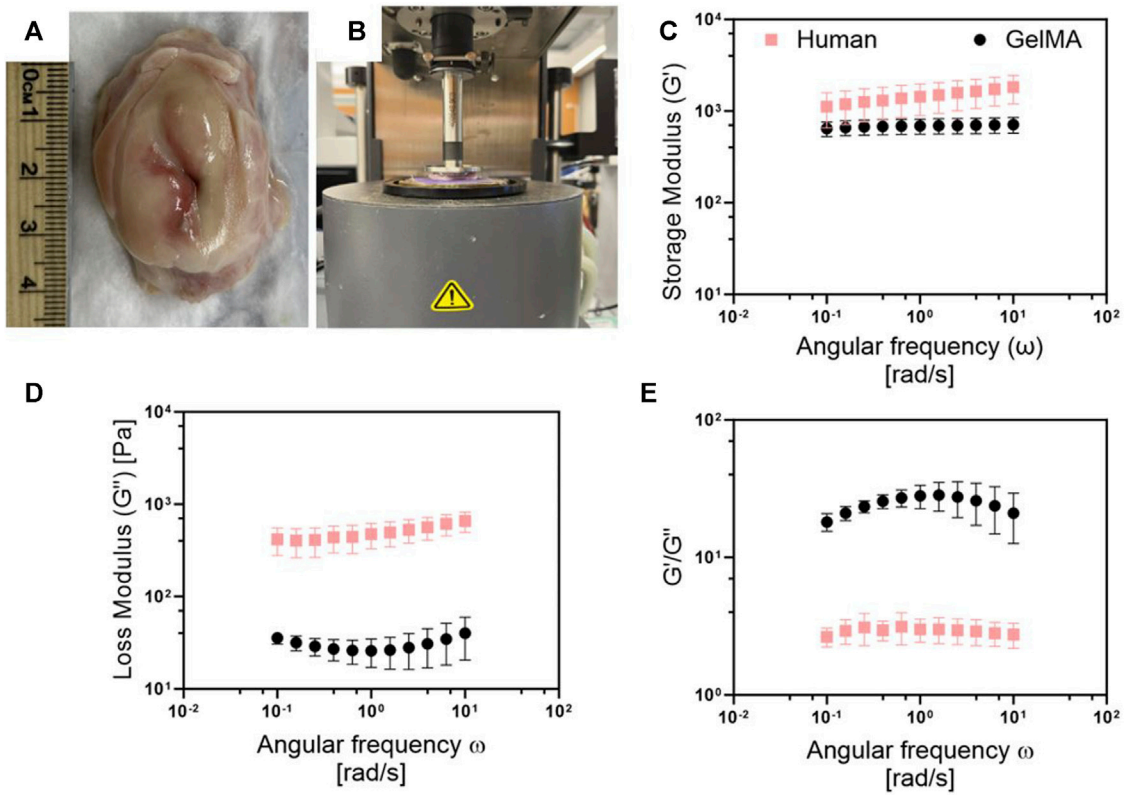

FIGURE 5
Comparison of the viscoelastic properties between the human cervix and Ge1MA. **(A)** Picture of human cervix obtained after autopsy from UMSOM. **(B)** Set up for rheornetric testing with AR-G2 rheometer. Comparison of **(C)** storage and **(D)** loss modulus, and **(E)** G′/G″ ratio of human cervices and Ge1MA hydrogel (8.7% w/v). Frequency sweeps were conducted from 0.1 to 100 rad/sec within the linear viscoelastic (LVE) region at a constant strain amplitude of 5%, and temperature of 37°C. Human cervix samples were stored in 10% PBS and incubated at 37°C for 1 h before experiments. Ge1MA hydrogels were crosslinked with LAP using a 405 nrn UV light source for about 1 min, then hydrogels were incubated at 37°C for 1-h prior measurement. Data represent the mean +SD (n = 5).

injection; as control, we cultured the 3D models in culture media (Figure 8A). After injection there was a significant decrease in cancer cell area in the 3D models treated with the EC-ethanol injection (Figure 8B), and 48 h post-injection the cancer cells were completely eliminated. In contrast, the SiHa cell area increased in the untreated control group. The cell area of fibroblasts and keratinocytes was also evaluated post-EC-ethanol injection. The area where the injection was applied caused a decrease in cell spread in all cell lines (Supplementary Figure S5). Outside the injection, we saw an increase in keratinocytes spreading, and the cell area for fibroblasts did not show a significant difference with the control group. Excitingly, there was no increase in SiHa cells outside of the injection site (Supplementary Figure S5). Taken together, these findings highlight the capacity of our model to provide a more comprehensive understanding of cellular reactions to the EC-ethanol injection and its efficacy in treating disease while preserving the surrounding healthy tissue.

4 Discussion

Current animal models face significant limitations in accurately replicating the intricate microenvironment characteristics of cervical dysplasia observed in humans (Larmour et al., 2015). *In vivo* models vary in human anatomy, physiology, and immune response, leading to disparities in disease modeling (Matchett et al., 2018). Animal models are often used due to the scarcity of human cervical tissue samples, but they fail to accurately represent the human cervical microenvironment. Additionally, animal models are unable to capture the complexity of human immune responses adequately, which is crucial to cervical dysplasia development, and variations in hormonal regulation between species can further impact disease progression (Ntuli et al., 2022). However, technical challenges in recreating the intricate microenvironment of cervical dysplasia in animal models result in oversimplified representations of the disease, further limiting their translational relevance to human patients (Malinowski, 2007). Recognizing this significant knowledge gap, we developed a 3D *in vitro* model to mimic the architectural complexity of cervical dysplasia, featuring a central region with cancer cells surrounded by healthy fibroblasts and keratinocytes. The development of our 3D *in vitro* model adds to the growing field of GelMA-based tissue-engineered models (Bupphathong et al., 2022). Our study represents a significant advancement in the field of cervical dysplasia research by introducing a novel 3D *in vitro* model that mimics the cellular and architectural complexity of cervical dysplasia. Furthermore, our work addresses several limitations of existing animal models, such as species differences and limited access to human samples, by providing a more accessible and reproducible experimental platform. Our innovative model aimed to

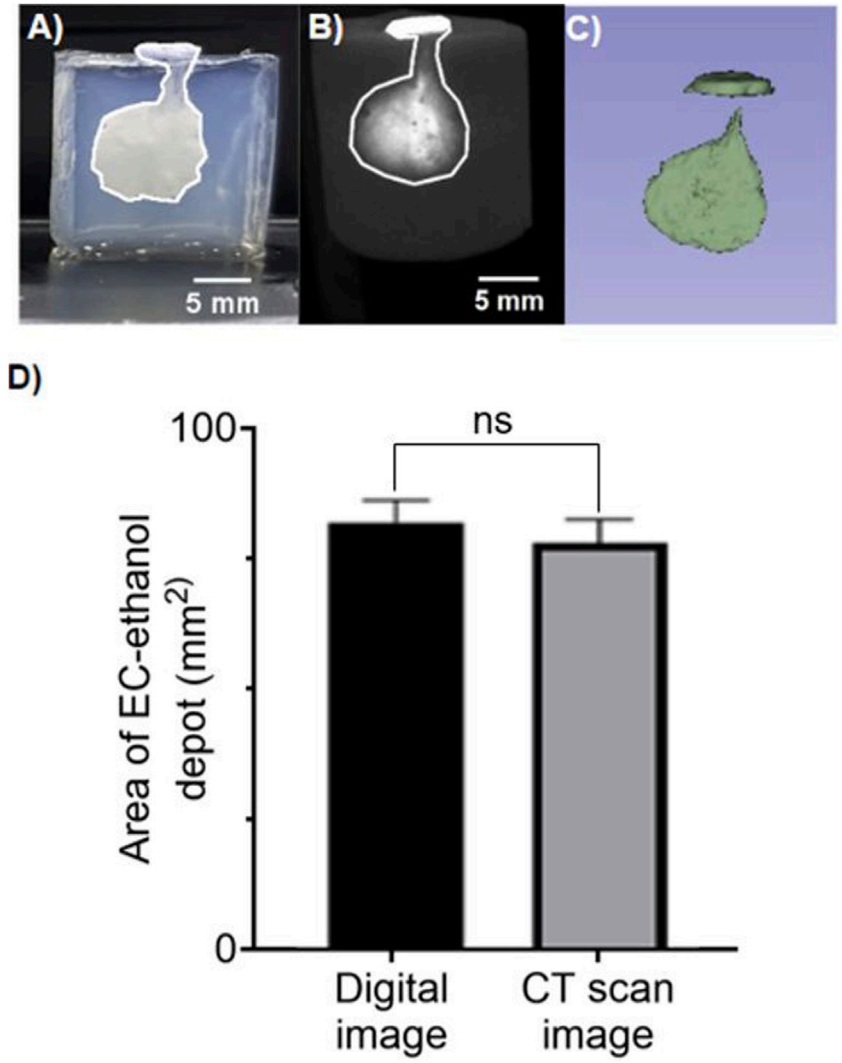

FIGURE 6
CT imaging to visualize distribution volume achieved with EC-Ethanol injection. Representative images of 12% EC- ethanol injections on 15 mm tall 8.7% GelMA hydrogels with Iohexol as a contrast agent. **(A)** Digital image of the EC-Ethanol gel depot with area of 86.93 mm^2. **(B)** Image acquired from CT imaging with area of 83.36 mm^2. **(C)** Coin shaped 3D projection of the depot acquired using 3D slicer. The following parameters were used: 22G - 25 mm-long beveled needles, 7 mm needle insertion depth, manual injection, 12% EC-ethanol, 80 mg/mL Iohexol. Images are shown as a side view. Scale bar = 5 mm. **(D)** Quantification of the cell area calculated from digital image vs. CT scan image. GelMA hydrogels were crosslinked with LAP using a 405 nm UV light source for about 1 min prior imaging. No statically significant differences were observed across the two group. Unpaired t-test. Data represent the mean ± SD (n = 5).

recapitulate the microenvironment of cervical lesions for evaluating the efficacy of ethyl cellulose (EC)-ethanol injection in mitigating cancer cell viability while preserving healthy tissue. Our 3D *in vitro* model is the first coculture system for cervical dysplasia in the literature and is the first to use an *in vitro* model to demonstrate EC-ethanol efficacy.

GelMA was selected as the supportive matrix for human fibroblast cells and cancer cells due to its biocompatibility and wide application in tissue engineering (Kim et al., 2022). We conducted a rheological characterization of the GelMA hydrogel formulation used in our model and compared its mechanical properties with human cervical tissue. It was confirmed that the GelMA hydrogel-based model demonstrated compatibility with human cervical tissue in terms of mechanical properties, and their values range in similar magnitudes to those observed in the literature (Dewall et al., 2010). Our results showed an average G′ of 1,453 Pa and a G″ of 494 Pa in the human cervix. Meanwhile, the GelMA hydrogel had a G′ of 686 Pa and a G″ of 30 Pa. Differences in the mechanical properties between our material and the human cervix are likely due to the ECM-components constituting the cervical tissue (Shi et al., 2022). However, the GelMA hydrogel has enough flexibility in its mechanical properties that allows the incorporation of more ECM components to approximate the human cervix better, a focus of future work (Nagaraj et al., 2022; Cadena et al., 2023).

Our GelMA-hydrogel model had high cell viability and promoted cell growth over 48 h. GelMA has proven to have good transport of nutrients and oxygen that enables cell response over time (Dong et al., 2022; Barros et al., 2023). A recent model showed

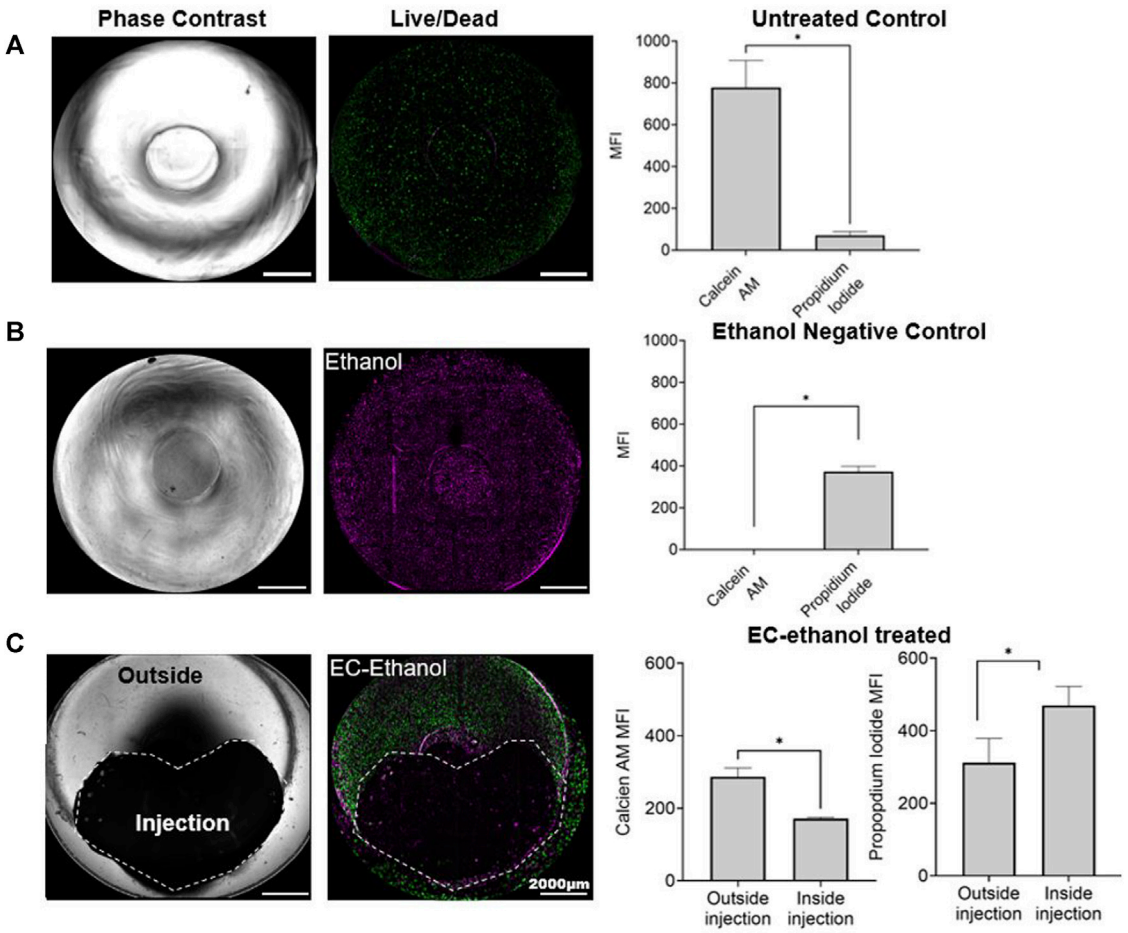

FIGURE 7
Effect of EC-ethanol on cell viability. 3D *in vitro* models **(A)** untreated and treated with **(B)** ethanol (99% v/v), and with **(C)** EC-ethanol injection. Representative images in bright field and with the fluorescent dies representing the live cells in green (Calcein AM) and the dead cells in magenta (propidium iodide). Data represent at 48 h post treatment. As control we culture the 3D *in vitro* model in **(A)** culture media, and **(B)** in ethanol for 48 h. The mean fluorescent intensity (MFI) of live cells (stained with calcein AM) and dead cell (stained with propidium iodide) was quantified using Fiji ImageJ. The scale bar was set at 2000 µm. Images were created and processed with Gen5 V3.14 software. 3D z-projections were generated using Fiji ImageJ. * $p < 0.05$, compared with the mean of each group. Paired t-test. Data represent the mean ± SD (n = 3).

the encapsulation of human pancreatic cells and stromal fibroblasts in GelMA (8% w/v) with the photoinitiator LAP could mimic cell-ECM interactions and is proven to have a good diffusion of nutrients and oxygen, which allowed the cells to proliferate in the GelMA beads (Huang et al., 2023). Using the GelMA hydrogel, we were able to increase the thickness of our first model and still have a higher number of live cells compared to dead cells. Moreover, in this study, we observed that cell viability and function were maintained in both models (10 mm and 15 mm), with the presence of healthy cells mostly on the outside and cancer cells on the inside. Over time, there was a slight spread of the cancer cells to the outside and an increase in cell area for the keratinocytes that were found in all the regions at 48 h.

To demonstrate a potential application of our 3D *in vitro* model, we evaluated the distribution area achieved with our EC-ethanol gel (through micro CT imaging) and the resulting region of cell viability and SiHa cell area post-injection. A critical finding of this work is that cell viability drastically decreased in the injection area while the outer region remained unaffected, suggesting the targeted, localized impact of EC-ethanol. As previously reported, studies suggested that a concentration higher than 6% of EC-ethanol gave a localized injection with minimal leakage and highlighted the potential of EC-ethanol in precisely targeting diseased areas (Morhard et al., 2020). The complement analysis on cell viability and cell area gave a better understanding of cell response to the EC-ethanol treatment in comparison with previous studies that have reported only the effect of the volume distribution of EC-ethanol (Morhard et al., 2020; Mueller et al., 2021). These findings highlight the nuanced and comprehensive understanding that our model offers regarding cellular reactions to EC-ethanol, emphasizing its promise as an ideal model in which to study the relationship between EC-ethanol distribution and cellular response. Moreover, our study demonstrates the efficacy of EC-ethanol in reducing cancer cell viability while preserving healthy tissue, highlighting the potential of this treatment approach for cervical dysplasia. In comparison to previous *in vitro* studies, which lack the 3D microenvironment or the interaction of healthy and disease cells in a complex coculture system (Aasen et al., 2003; Bonartsev et al., 2022), our 3D *in vitro* model better mimicked the cervical microenvironment and uniquely enabled visualization of the EC-ethanol treatment in 3D. We observed a significant decrease in the SiHa cell area following the

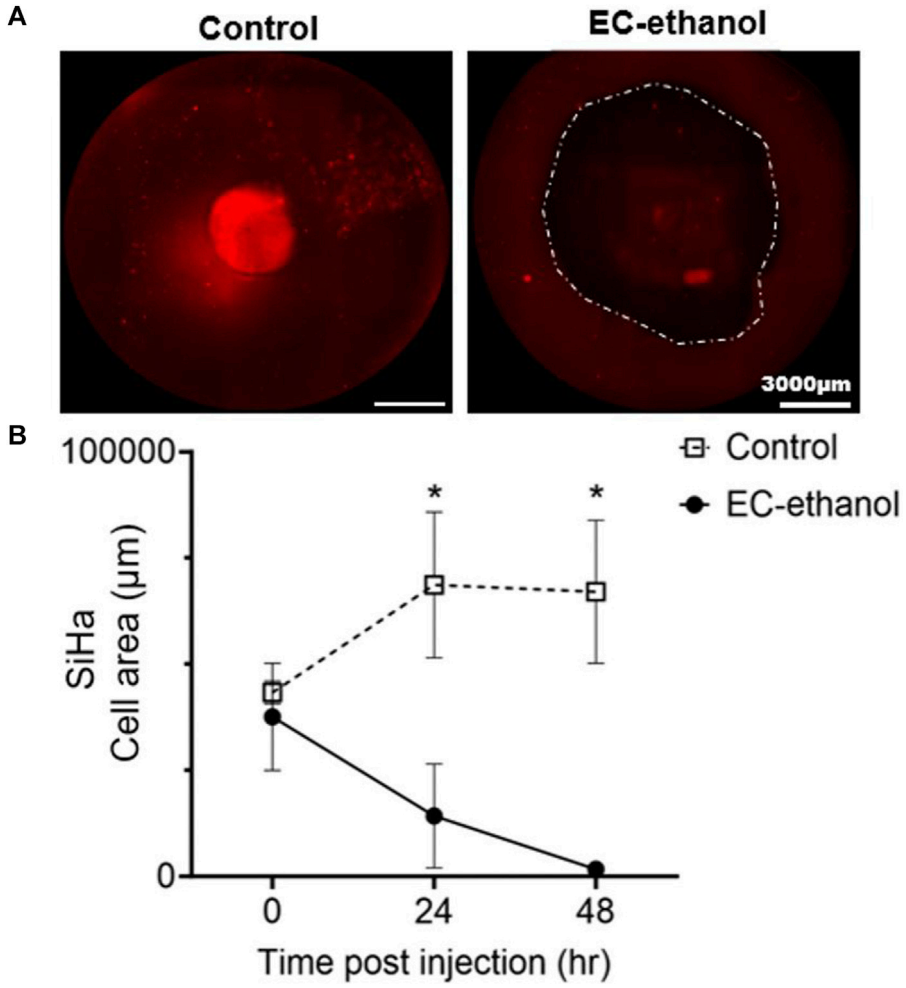

FIGURE 8
Effect of EC-ethanol on SiHa cell area. **(A)** Representative images of SiHa cells (CellTracker Red-labeled) cultured in 3D *in vitro* model at 48 h with and without EC- ethanol injection. A 2D z-projection of full construct was created using Gen5 V3.14 software to quantify the SiHa cell area post- EC ethanol treatment. Dash line shows the area were the EC-ethanol injection was applied after 48 h of cocultured. **(B)** SiHa cell area at all time points pre (time 0) and post injection (24 h and 48 h). Cell area was tracked by staining SiHa cells with CellTracker Red CMTPX (C34552). The scale bar was set at 3000 μm. Images were created and processed with Gen5 V3.14 software. SiHa cell area was quantified using Fiji ImageJ. * $p < 0.05$, compared to the EC-ethanol group. Control group had only culture media. Two-way ANOVA with Tukey post-test. Data represent the mean ± SD (n = 4).

injection of EC-ethanol. However, the surroundings of the injection preserved or maintained healthy cell growth while decreasing the spread of SiHa cells. Due to the paucity of animal models of cervical dysplasia, we had previously evaluated EC-ethanol in a normal swine cervix model, which was not diseased. These *in vitro* results mirror those observed in the swine model in terms of local delivery (Quang et al., 2023). However, here, for the first time, we are able to assess whether or not the diseased lesions were removed in a human-sized model of cervical dysplasia. Our study showed that the 3D model was able to capture the target cancer cell effect while preserving the healthy cells that were outside the site of injection. Overall, our study has the potential to significantly impact the field of cervical dysplasia research and to pave the way for the development of more effective therapeutic strategies.

Our study presents an innovative approach to address the drawbacks of existing animal models for studying cervical dysplasia. However there were several limitations of this study. While our 3D *in vitro* model mimics the architectural complexity of cervical dysplasia, it may still lack some key features of the *in vivo* microenvironment, such as immune cell infiltration, interactions with surrounding tissues and the addition of ECM components involved in disease progression (Sobel et al., 2005). Incorporating additional components, such as immune cells and endothelial cells, into the 3D *in vitro* model can better simulate the complex interactions present in the disease. Additionally, although GelMA hydrogel has shown good biocompatibility and mechanical properties comparable to human cervical tissue, its composition may not fully replicate the ECM components present in cervical tissue, potentially influencing cellular behavior and response to treatment. We have previously reported changes in mechanical properties by combining GelMA with collagen type I and fibronectin. Our hydrogel formulation significantly enhanced cervical cancer invasion over time compared to Matrigel and GelMA alone (Cadena et al., 2023). Adding similar components to the presented 3D model, but in a concentration range for cervical dysplasia, could open the opportunity to better mimic cell adhesion and cell-ECM crosstalk in the 3D *in vitro* model. Moreover,

further studies with the inclusion of ECM components could delve into the molecular mechanisms underpinning these observed effects, further advancing our understanding of how to best deliver EC-ethanol to treat cervical dysplasia. One issue that may be encountered with scaling up the 3D *in vitro* model with more ECM components is the hypoxia effect for cells located in the core in the long-term utilization of the model, which can be addressed by modulating the cell density and incorporating vascularization within the model to enhance oxygen transport and nutrient delivery. Although our study demonstrated the efficacy of EC-ethanol in reducing cancer cell viability in the injected area while preserving healthy tissue, the long-term effects and potential systemic impact of this treatment are yet to be studied. Future studies aim to address these limitations by incorporating additional components of the cervical microenvironment and investigating the broader physiological implications of EC-ethanol treatment.

5 Conclusion

We developed a 3D *in vitro* model of cervical dysplasia that demonstrated the successful elimination of cervical dysplasia following EC-ethanol injection while leaving the surrounding healthy cells intact. These results show the promise of using our 3D *in vitro* model to study localized interventions in cervical dysplasia, and the insights gained from EC-ethanol ablation in the 3D *in vitro* model will inform its future *in vivo* applications. While our initial findings are promising for treating lesions, critical questions remain regarding optimal delivery parameters, particularly as lesions progress from low-grade to high-grade dysplasia to early invasive disease. These parameters are pivotal for the effective delivery of EC-ethanol into the cervix, ensuring comprehensive coverage of precancerous lesions and early invasive disease within deeper tissue layers. Further investigation of these delivery parameters is essential for the successful translation of EC-ethanol and similar therapeutic solutions for treating cervical dysplasia in LMICs.

Data availability statement

The datasets presented in this study can be found in online repositories. The names of the repository/repositories and accession number(s) can be found in the article/Supplementary Material.

Author contributions

IC: Conceptualization, Data curation, Project administration, Resources, Supervision, Visualization, Writing–original draft, Writing–review and editing, Formal Analysis, Investigation, Methodology, Software, Validation. GA: Conceptualization, Data curation, Formal Analysis, Investigation, Methodology, Project administration, Resources, Software, Supervision, Validation, Visualization, Writing–original draft, Writing–review and editing. AA: Formal Analysis, Methodology, Validation, Writing–original draft, Writing–review and editing. MJ: Formal Analysis, Writing–original draft, Writing–review and editing, Data curation. NO: Data curation, Formal Analysis, Writing–original draft, Writing–review and editing. NS: Writing–original draft, Writing–review and editing, Investigation, Software. WR: Writing–original draft, Writing–review and editing, Data curation. JM: Methodology, Project administration, Resources, Supervision, Visualization, Writing–original draft, Writing–review and editing, Conceptualization, Formal Analysis, Funding acquisition. KF: Conceptualization, Funding acquisition, Project administration, Resources, Supervision, Visualization, Writing–original draft, Writing–review and editing, Data curation.

Funding

The author(s) declare that financial support was received for the research, authorship, and/or publication of this article. This work was supported by Oregon State University startup funds (KF), and the University of Maryland startup funds (JM).

Conflict of interest

IC, GA, JM, and KF have filed a provisional patent related to this work. The remaining authors declare that the research was conducted in the absence of any commercial or financial relationships that could be construed as a potential conflict of interest.

Publisher's note

Supplementary material

The Supplementary Material for this article can be found online at: https://www.frontiersin.org/articles/10.3389/fbiom.2024.1365781/full#supplementary-material

References

Aasen, T., Hodgins, M. B., Edward, M., and Graham, S. V. (2003). The relationship between connexins, gap junctions, tissue architecture and tumour invasion, as studied in a novel *in vitro* model of HPV-16-associated cervical cancer progression. *Oncogene* 22, 7969–7980. doi:10.1038/sj.onc.1206709

Abdul-Karim, F. W., Fu, Y. S., Reagan, J. W., and Wentz, W. B. (1982). Morphometric study of intraepithelial neoplasia of the uterine cervix. *Obstet. Gynecol.* 60 (2), 210–214.

Adhikari, G., Sarojasamhita, V. P., Richardson-Powell, V., Farooqui, A., Budzinski, M., Garvey, D. T., et al. (2023). Impact of injection-based delivery parameters on local

distribution volume of EthylCellulose ethanol gel in tissue and tissue mimicking phantoms. *IEEE Trans. Biomed. Eng.*, 1–11. doi:10.1109/tbme.2023.3340613

Belair, D. G., and Abbott, B. D. (2017). Engineering epithelial-stromal interactions in vitro for toxicology assessment. *Toxicology* 382, 93–107. doi:10.1016/j.tox.2017.03.007

Barros, N. R., Gomez, A., Ermis, M., Falcone, N., Haghniaz, R., Young, P., et al. (2023). Gelatin methacryloyl and Laponite bioink for 3D bioprinted organotypic tumor modeling. *Biofabrication* 15 (4), 045005. doi:10.1088/1758-5090/ace0db

Bogorad, M. I., Karlsson, J., Wong, A. D., Gerecht, S., and Searson, P. C. (2015). Review: in vitro microvessel models. *Lab Chip* 15, 4242–4255. doi:10.1039/C5LC00832H

Bonartsev, A. P., Lei, B., Kholina, M.S., Menshikh, K. A., Svyatoslavov, D. S., Samoylova, S. I., et al. (2022). Models of head and neck squamous cell carcinoma using bioengineering approaches. *Crit Rev Oncol Hematol* 175, 103724. doi:10.1016/j.critrevonc.2022.103724

Cadena, I. A., Buchanan, M. R., Harris, C. G., Jenne, M. A., Rochefort, W. E., Nelson, D., et al. (2023). Engineering high throughput screening platforms of cervical cancer. *J. Biomed. Mater. Res. Part A* 111 (6), 747–764. doi:10.1002/jbm.a.37522

Comprehensive Cervical Cancer Control (2014). *Comprehensive cervical cancer control: a guide to essential practice*. 2nd ed. Geneva: World Health Organization. Available at: http://www.ncbi.nlm.nih.gov/books/NBK269619/.

De Gregorio, V., Urciuolo, F., Netti, P. A., and Imparato, G. (2020). *In vitro* organotypic systems to model tumor microenvironment in human papillomavirus (HPV)-Related cancers. *Cancers* 12 (5), 1150. doi:10.3390/cancers12051150

Dewall, R. J., Varghese, T., Kliewer, M. A., Harter, J. M., and Hartenbach, E. M. (2010). Compression-dependent viscoelastic behavior of human cervix tissue. *Ultrason. Imaging* 32 (4), 214–228. doi:10.1177/016173461003200402

Dong, Y., Zhang, M., Han, D., Deng, Z., Cao, X., Tian, J., et al. (2022). A high-performance GelMA-GelMA homogeneous double-network hydrogel assisted by 3D printing. *J. Mater Chem. B* 10 (20), 3906–3915. doi:10.1039/d2tb00330a

Ferlay, J., Soerjomataram, I., Dikshit, R., Eser, S., Mathers, C., Rebelo, M., et al. (2015). Cancer incidence and mortality worldwide: sources, methods and major patterns in GLOBOCAN 2012. *Int. J. Cancer* 136 (5), E359–E386. doi:10.1002/ijc.29210

Gage, J. C., Ferreccio, C., Gonzales, M., Arroyo, R., Huivín, M., and Robles, S. C. (2003). Follow-up care of women with an abnormal cytology in a low-resource setting. *Cancer Detect Prev.* 27 (6), 466–471. doi:10.1016/j.cdp.2003.09.004

Huang, B., Wei, X., Chen, K., Wang, L., and Xu, M. (2023). Bioprinting of hydrogel beads to engineer pancreatic tumor-stroma microtissues for drug screening. *Int. J. Bioprint* 9 (3), 676. doi:10.18063/ijb.v9i3.676

Huchko, M. J., Sneden, J., Leslie, H. H., Abdulrahim, N., Maloba, M., Bukusi, E., et al. (2014). A comparison of two visual inspection methods for cervical cancer screening among HIV-infected women in Kenya. *Bull. World Health Organ* 92 (3), 195–203. doi:10.2471/blt.13.122051

Huchko, M. J., Sneden, J., Zakaras, J. M., Smith-McCune, K., Sawaya, G., Maloba, M., et al. (2015). A randomized trial comparing the diagnostic accuracy of visual inspection with acetic acid to visual inspection with lugol's iodine for cervical cancer screening in HIV-infected women. *PLoS One* 10 (4), e0118568. doi:10.1371/journal.pone.0118568

Human papillomavirus vaccines (2015). Human papillomavirus vaccines: WHO position paper, October 2014-Recommendations. *Vaccine* 33 (36), 4383–4384. doi:10.1016/j.vaccine.2014.12.002

Jeronimo, J., Morales, O., Horna, J., Pariona, J., Manrique, J., Rubiños, J., et al. (2005). Visual inspection with acetic acid for cervical cancer screening outside of low-resource settings. *Rev. Panam. Salud Publica* 17 (1), 1–5. doi:10.1590/s1020-49892005000100001

Kim, Y. H., Dawson, J. I., Oreffo, R. O. C., Tabata, Y., Kumar, D., Aparicio, C., et al. (2022). Gelatin methacryloyl hydrogels for musculoskeletal tissue regeneration. *Bioeng. (Basel)* 9 (7), 332. doi:10.3390/bioengineering9070332

Lam, C. T., Krieger, M. S., Gallagher, J. E., Asma, B., Muasher, L. C., Schmitt, J. W., et al. (2015). Design of a novel low-cost point of care tampon (POCkeT) colposcope for use in resource-limited settings. *PLOS ONE* 10 (9), e0135869. doi:10.1371/journal.pone.0135869

Larmour, L. I., Jobling, T. W., and Gargett, C. E. (2015). A review of current animal models for the study of cervical dysplasia and cervical carcinoma. *Int. J. Gynecol. Cancer* 25 (8), 1345–1352. doi:10.1097/igc.0000000000000525

Lorenzen, E., Follmann, F., Jungersen, G., and Agerholm, J. S. (2015). A review of the human vs. porcine female genital tract and associated immune system in the perspective of using minipigs as a model of human genital Chlamydia infection. *Veterinary Res.* 46 (1), 116. doi:10.1186/s13567-015-0241-9

Malinowski, D. P. (2007). Multiple biomarkers in molecular oncology. I. Molecular diagnostics applications in cervical cancer detection. *Expert Rev Mol Diagn* 7, 117–131. doi:10.1586/14737159.7.2.117

Matchett, W. E., Anguiano-Zarate, S. S., and Barry, M. A. (2018). Comparison of systemic and mucosal immunization with replicating Single cycle Adenoviruses. *Glob Vaccines Immunol* 3, doi:10.15761/GVI.1000128

Montazerian, H., Baidya, A., Haghniaz, R., Davoodi, E., Ahadian, S., Annabi, N., et al. (2021). Stretchable and bioadhesive gelatin methacryloyl-based hydrogels enabled by *in situ* dopamine polymerization. *ACS Appl. Mater Interfaces* 13 (34), 40290–40301. doi:10.1021/acsami.1c10048

Morhard, R., Mueller, J. L., Tang, Q., Nief, C., Chelales, E., Lam, C. T., et al. (2020). Understanding factors governing distribution volume of ethyl cellulose-ethanol to optimize ablative therapy in the liver. *IEEE Trans. Biomed. Eng.* 67 (8), 2337–2348. doi:10.1109/tbme.2019.2960049

Morhard, R., Nief, C., Barrero Castedo, C., Hu, F., Madonna, M., Mueller, J. L., et al. (2017). Development of enhanced ethanol ablation as an alternative to surgery in treatment of superficial solid tumors. *Sci. Rep.* 7 (1), 8750. doi:10.1038/s41598-017-09371-2

Mueller, J. L., Asma, E., Lam, C. T., Krieger, M. S., Gallagher, J. E., Erkanli, A., et al. (2017). International image concordance study to compare a point-of-care tampon colposcope with a standard-of-care colposcope. *J. Low. Genit. Tract. Dis.* 21 (2), 112–119. doi:10.1097/lgt.0000000000000306

Mueller, J. L., Lam, C. T., Dahl, D., Asiedu, M. N., Krieger, M. S., Bellido-Fuentes, Y., et al. (2018). Portable Pocket colposcopy performs comparably to standard-of-care clinical colposcopy using acetic acid and Lugol's iodine as contrast mediators: an investigational study in Peru. *BJOG* 125 (10), 1321–1329. doi:10.1111/1471-0528.15326

Mueller, J. L., Morhard, R., DeSoto, M., Chelales, E., Yang, J., Nief, C., et al. (2021). Optimizing ethyl cellulose-ethanol delivery towards enabling ablation of cervical dysplasia. *Sci. Rep.* 11 (1), 16869. doi:10.1038/s41598-021-96223-9

Muñoz, N. M., Williams, M., Dixon, K., Dupuis, C., McWatters, A., Avritscher, R., et al. (2021). Influence of injection technique, drug formulation and tumor microenvironment on intratumoral immunotherapy delivery and efficacy. *J. Immunother. Cancer* 9 (2), e001800. doi:10.1136/jitc-2020-001800

Nagaraj, A., Etxeberria, A. E., Naffa, R., Zidan, G., and Seyfoddin, A. (2022). 3D-Printed hybrid collagen/GelMA hydrogels for tissue engineering applications. *Biol. (Basel).* 11 (11), 1561. doi:10.3390/biology11111561

Nichol, J. W., Koshy, S., Bae, H., Hwang, C. M., Yamanlar, S., Khademhosseini, A., et al. (2010). Cell-laden microengineered gelatin methacrylate hydrogels. *Biomaterials* 31, 5536–5544. doi:10.1016/j.biomaterials.2010.03.064

Nief, C., Morhard, R., Chelales, E., Alvarez, D. A., Bs, I. B., Lam, C. T., et al. (2021). Polymer-assisted intratumoral delivery of ethanol: preclinical investigation of safety and efficacy in a murine breast cancer model. *PLOS ONE* 16 (1), e0234535. doi:10.1371/journal.pone.0234535

Ntuli, L., Mtshali, A., Mzobe, G., Liebenberg, L. J., and Ngcapu, S. (2022). Role of Immunity and Vaginal Microbiome in Clearance and Persistence of Human Papillomavirus Infection. *Front. Cell. Infect. Microbiol.* 12. doi:10.3389/fcimb.2022.927131

Path (2013). Cervical cancer screening and treatment in low-resource settings: practical experience from PATH. Available at: https://www.path.org/resources/cervical-cancer-screening-and-treatment-in-low-resource-settings-practical-experience-from-path/.

Quang, T. T., Yang, J., Kaluzienski, M. L., Parrish, A., Farooqui, A., Katz, D., et al. (2023). *In Vivo* Evaluation of Safety and Efficacy of Ethyl Cellulose-Ethanol Tissue Ablation in a Swine Cervix Model. *Bioengineering (Basel)* 10, 1246. doi:10.3390/bioengineering10111246

Seki, T., Nonaka, T., Kubota, Y., Mizuno, T., and Sameshima, Y. (1989). Ultrasonically guided percutaneous ethanol injection therapy for hepatocellular carcinoma. *Am. J. Gastroenterol.* 84 (11), 1400–1407.

Shi, L., Hu, L., Lee, N., Fang, S., and Myers, K. (2022). Three-dimensional anisotropic hyperelastic constitutive model describing the mechanical response of human and mouse cervix. *Acta Biomater.* 150, 277–294. doi:10.1016/j.actbio.2022.07.062

Sobel, G., Szabó, I., Páska, C., Kiss, A., Kovalszky, I., Kádár, A., et al. (2005). Changes of cell adhesion and extracellular matrix (ECM) components in cervical intraepithelial neoplasia. *Pathol Oncol Res* 11, 26–31. doi:10.1007/BF03032402

Tsu, V. D., Jeronimo, J., and Anderson, B. O. (2013). Why the time is right to tackle breast and cervical cancer in low-resource settings. *Bull. World Health Organ* 91 (9), 683–690. doi:10.2471/blt.12.116020

Van Den Bulcke, A. I., Bogdanov, B., De Rooze, N., Schacht, E. H., Cornelissen, M., and Berghmans, H. (2000). Structural and rheological properties of methacrylamide modified gelatin hydrogels. *Biomacromolecules* 1, 31–38. doi:10.1021/bm990017d

Xu, H., Casillas, J., Krishnamoorthy, S., and Xu, C. (2020). Effects of Irgacure 2959 and lithium phenyl-2,4,6-trimethylbenzoylphosphinate on cell viability, physical properties, and microstructure in 3D bioprinting of vascular-like constructs. *Biomed. Mater* 15 (5), 055021. doi:10.1088/1748-605x/ab954e

Yue, K., Trujillo-de Santiago, G., Alvarez, M. M., Tamayol, A., Annabi, N., and Khademhosseini, A. (2015). Synthesis, properties, and biomedical applications of gelatin methacryloyl (GelMA) hydrogels. *Biomaterials* 73, 254–271. doi:10.1016/j.biomaterials.2015.08.045